Characterization of Chemical Exchange between Soluble and Aggregated States of β-Amyloid by Solution-State NMR upon Variation of Salt Conditions†

Saravanakumar Narayanan‡,§ and Bernd Reif*,‡,||

Forschungsinstitut für Molekulare Pharmakologie (FMP), Robert-Rössle-Strasse 10, D-13125 Berlin, Germany, and Charite Universitätsmedizin, D-10117 Berlin, Germany

Received August 12, 2004; Revised Manuscript Received November 13, 2004

ABSTRACT: Alzheimer's disease (AD) is characterized by the accumulation of insoluble fibrillar aggregates of β-amyloid peptides (Aβ), a 39−42 residue peptide, in the brain of AD patients. It is hypothesized that the disease causing form is not the fibrillar species but an oligomeric Aβ molecule, which is often referred to as the "critical oligomer" of Aβ. We show in this paper that Aβ^{1-40} undergoes chemical exchange between a monomeric, soluble state and an oligomeric, aggregated state under physiological conditions. In circular dichroism spectroscopy, we observe for this intermediate an α-helical structure. The oligomer is assigned a molecular weight of >100 kDa by diffusion-ordered spectroscopy−solution-state NMR spectroscopy (NMR). We can show by saturation transfer difference NMR experiments that the oligomer is related to monomeric Aβ. This experiment also allows us to identify the chemical groups that are involved in interactions between mono- and oligomeric Aβ molecules. Variation of the anionic strength in the buffer induces a shift of equilibrium between mono- and oligomeric states and possibly allows for the stabilization of these intermediate structures.

Alzheimer's disease (AD)[1] is the most abundant age-related neurodegenerative disease. The β-amyloid peptide (Aβ), which exists in different lengths (39−43 amino acids), is generated after processing of a transmembrane protein, APP (*1*, *2*). The disease is characterized by two fundamental events, the accumulation of insoluble fibrillar aggregates of Aβ and the degeneration and death of neurons in the brain regions that are concerned with learning and memory processes. Abnormal protein deposition is also a shared characteristic of other age-related neurodegenerative diseases, such as Parkinson's disease, Huntington's disease, and the prion diseases. There is increasing evidence that the mechanism of this aggregation may be similar in each of these diseases (*3*). At the same time, it is found that probably not the fibrillar state but a protofibrillar state is responsible for neurotoxicity (*4*−*6*). Most interestingly, it was found recently that antibodies can specifically recognize these soluble oligomers (*7*). So far, the molecular basis for the neurotoxicity of Aβ could not be identified. It is speculated that Aβ^{1-40} forms a pore in the membrane and leads to a unregulated flux of Ca^{2+} in and out of the cell (*6*). Alternatively, Aβ^{1-40} may generate radicals that are neurotoxic themselves (*8*−*10*). However, it is not understood why only certain aggregation states of Aβ^{1-40} should be associated with neurotoxicity given the identical primary structure of Aβ^{1-40}. So far, NMR structural studies of Aβ^{1-40} show that the peptide is mostly unstructured in aqueous solution (*11*, *12*). It was shown as well that Aβ^{1-40} adopts a helix-turn-helix structure upon addition of tetrafluoroethylene (*13*, *14*) or sodium dodecyl sulfate (SDS) (*15*, *16*). Recently, also solid-state NMR structural data is available for Aβ^{1-40} in the fibrillized state (*17*). Interestingly, a similar loop at approximately the same position in the primary structure was found around residues S^{26}NKG, which was already observed in the SDS solution-state structure (*15*). In the solid-state structure, the only charged side chains in the core are those of D23 and K28, which form a salt bridge (*17*). The C terminus of the peptide folds back onto the hydrophobic core, so that the hydrophobic core and the aliphatic side chains of the C terminus come in close contact.

The goal of the proposed NMR experiments is to find solution conditions that possibly allow for the study of different intermediates in the Aβ aggregation process. In addition, we aimed to characterize the chemical groups of Aβ^{1-40}, which are involved in peptide−peptide interactions during aggregation. Knowledge of these interactions might possibly show avenues to prevent accumulation of a neurotoxic, oligomeric intermediate. We want to answer this question by performing a series of saturation transfer difference (STD) experiments. STD experiments have been introduced recently to screen compound mixtures for binding

† This research was supported by a Grant of the Deutsche Forschungsgemeinschaft (DFG), Re1435/2.

* To whom correspondence should be addressed. Telephone: +49(30)94793-191. Fax: +49(30)94793-199. E-mail: reif@fmp-berlin.de.

‡ Forschungsinstitut für Molekulare Pharmakologie (FMP).

§ Institut für Organische Chemie und Biochemie II, TU München, Lichtenbergstrasse 4, D-85747 Garching, Germany.

|| Charité Universitätsmedizin.

[1] Abbreviations: Aβ, human β-amyloid peptide; AD, Alzheimer's disease; APP, amyloid precursor protein; CD, circular dichroism; DOSY, diffusion-ordered spectroscopy; LMW, low molecular weight; NMR, solution-state NMR spectroscopy; PBS, phosphate-buffered saline; STD, saturation transfer difference.

10.1021/bi048264b CCC: $30.25
Published on Web 01/08/2005

to a receptor protein (*18*) and to characterize interactions between membrane channel proteins and neurotoxic peptides (*19*). Recently, we have shown that this method can also be applied to characterize the interaction between a yeast prion protein Sup35 and Hsp104 under nonequilibrium conditions (*20*).

MATERIALS AND METHODS

Peptide Synthesis and Protein Preparation. $A\beta^{1-40}$ was obtained from Biosource International, Camrillo, CA. The sample buffer contained 50 mM phosphate at pH 6.9. In addition, a varying amount of sodium sulfate or sodium chloride was added to the buffer as mentioned in the text. A concentration of $A\beta^{1-40}$ of 0.5 mM was used in the NMR experiments. $A\beta^{1-40}$ was directly dissolved in 450 μL of buffer and 50 μL of D_2O. No attempt was made to dissolve possible aggregates before starting the experiment. In all samples, β-mercaptoethanol was added at a concentration of 200 μM as an internal standard for the DOSY experiments. Care was taken to reproduce the same peptide concentration in all NMR experiments. The error in balancing $A\beta^{1-40}$ is estimated to be on the order of 5%. To determine the solubility of the sample, the signal-to-noise (S/N) ratio of the $A\beta^{1-40}$ solution (0.5 mM, 50 mM phosphate at pH 6.9 and 50 mM NaCl) is compared with an external standard (glutathion). We find that the soluble fraction of the $A\beta^{1-40}$ solution amounts to approximately 70%. The S/N ratio was calibrated using a 500 μL sample of a 1 mM glutathione solution (in 50 mM phosphate at pH 6.9) as a reference. Both samples were measured using the same experimental parameters, spectrometer, and probe. The data were processed in such a way that line-width effects on the intensity of the signal are negligible. In our hands, it was not possible to dissolve $A\beta$ directly in phosphate buffer containing no additional salt. To obtain an $A\beta$ sample with 0 mM NaCl, a solution containing 50 mM NaCl was dialyzed overnight against a solution containing only phosphate buffer.

Solution-State NMR Spectroscopy (NMR): Diffusion-Ordered Spectroscopy (DOSY). DOSY−NMR (*21*) were carried out to determine the molecular weight of $A\beta^{1-40}$. In these experiments, the size of a molecule can be estimated by encoding the diffusion of a molecule in a gradient echo. The measured diffusion constant $D = (k_B T)/(6\pi\eta F r_S)$ is related via the Stokes−Einstein relation to the hydrodynamic radius r_S of the molecule, and, thus, to the molecular weight at a given viscosity η of the solution. k_B denotes Boltzmann's constant; T, the absolute temperature; and F, the dimensionless Perrin factor. Only molecules that are not diffusing along a given axis are detected. The decay of magnetization can be analyzed in an analytical way, employing $I/I_0 = \exp\{-D(\Delta-\delta/3)q^2\}$, where $q = \gamma\delta g$. Δ refers to the separation of the gradient echo; δ, to the duration of the gradient; γ, to the gyromagnetic ratio of the nucleus; and g, to the strength of the gradient. Pulsed-field gradient (PFG) experiments with water-suppressed longitudinal encoding decoding (water-sLED) pulses (*22*) were performed to determine the relative oligomeric state of the β-amyloid peptide using the internal standard method (*23*). In the experiment, the duration of the gradients was set to 2.0 ms; 30.0 ms was used as delay to allow for diffusion between the dephasing and rephasing gradient, and 32 points have been recorded in the indirect dimension. Sine-shaped gradients and a gradient ramp with a maximum gradient strength of 35 G/cm were employed. Gradient strengths are always given in percent squared with respect to maximum gradient strength (100% = 35 G/cm). A buffer resonance (oxidized β-mercaptoethanol, M_r = 156 Da) was used as an internal reference to calculate the molecular mass of the amyloid oligomers.

STD. STD was successfully used in the past to screen compound mixtures for binding to a receptor protein (*18*, *19*, *24*). Furthermore, it was used to characterize interactions between membrane channel proteins and neurotoxic peptides (*19*, *25*). This way, it is possible to identify the chemical groups involved in ligand binding. The experiment relies on the selective saturation of the ^{1}H resonances of a target protein. If a ligand binds weakly, saturation is transferred via cross relaxation to the bound ligand. An attenuated signal is then observed for the free ligand after dissociation. Higher STD intensites correspond to group epitopes, which are closer in space with respect to the binding site in the (aggregated) target molecule. The method works best for small ligands (with fast correlation times) and large complexes, where the reorientation process is slow enough to give rise to large cross-relaxation rates. Experimentally, a train of 300 square pulses of 12 ms duration (with a 1.0 ms gap between the pulses) is applied to saturate the ^{1}H(methyl) resonances of the amyloid aggregates. Even (on-resonance irradiation at −0.02 ppm) and odd (off-resonance irradiation at +30.0 ppm) scans are recorded subsequently and subtracted from each other by incrementation of the receiver phase. A total of 512 scans are accumulated for each one-dimensional (1D) experiment, resulting in a total experimental time of 45 min. STD experiments have always been adjusted in the first place in a reference experiment on a sample containing a reference peptide (LPFFD and $Sup35^{5-26}$) to minimize artifacts.

RESULTS

We searched for (physiological) solution-state conditions that would possibly allow for the shifting of the chemical equilibrium between different aggregation states of $A\beta^{1-40}$. Goto and Aimoto (*26*) could show by circular dichroism (CD) spectroscopy that addition of anions to the buffer solution can induce α-helical structure in otherwise unstructured amphiphilic polypeptides. The stabilization is proportional to the strength of the anion added in the order of triphosphate^{4-} > diphosphate^{3-} > phosphate^{2-} > SO_4^{2-} > ClO_4^- > Cl^- > F^-. An increase in propensity for the α-helical structure in $A\beta^{1-40}$ should, in analogy to the results obtained by Goto and Aimoto, decrease the propensity for amyloid-aggregate formation. We added 100 mM F^-, Cl^-, NO_3^-, ClO_4^-, and SO_4^{2-} to the buffer solution and observed an increase in solubility for $A\beta^{1-40}$ in the order indicated (data not shown).

The CD spectrum displays a decrease of contributions, which are due to a random coil upon increase of the anionic strength (Figure 1a). At the same time, the amount of contributions of α-helical secondary-structure elements is increased. The quantitative distribution of secondary-structure elements is represented in Table 1. For the fitting of the CD curves, CDSSTR and CONTINLL were employed (*27*).

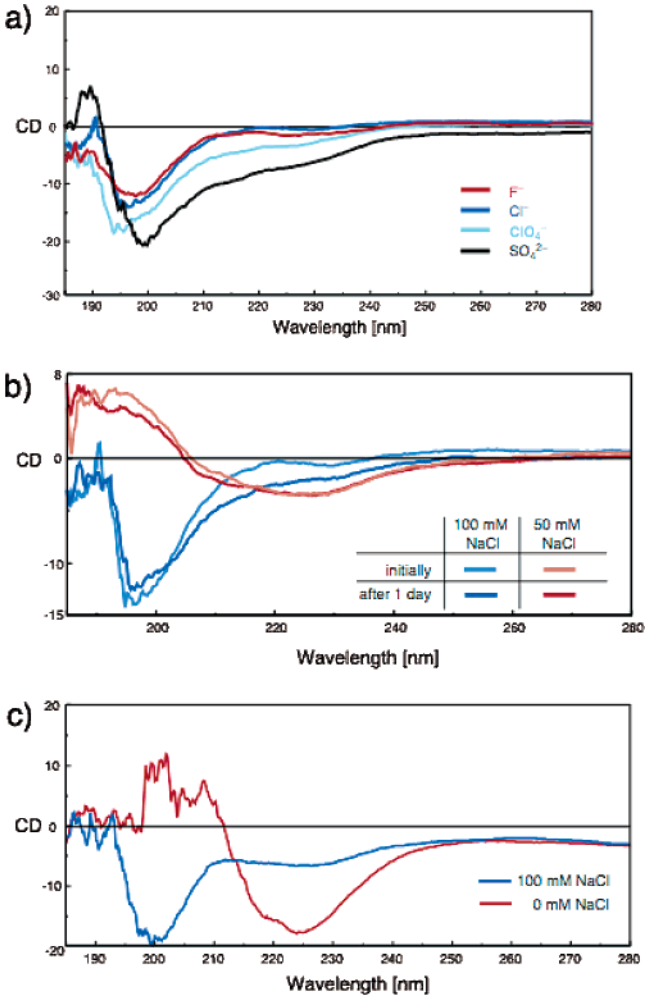

FIGURE 1: (a) CD spectra of a 0.15 mM Aβ^{1-40} dissolved in buffer solution with additional 100 mM salt. NaF (red), NaCl (dark blue), $NaClO_4$ (light blue), and Na_2SO_4 (black). The sample was filtered through a membrane with a 0.2 μm pore diameter before transfer into the CD cuvette. (b) CD spectra of a 0.15 mM Aβ^{1-40} solution employing a salt concentration of 50 mM NaCl (red) and 100 mM NaCl (blue). In contrast to a, the spectra were obtained without filtering the sample prior to the measurement. This preparation is analogous to the NMR sample preparation. (c) CD spectra of a 0.50 mM Aβ^{1-40} solution employing a salt concentration of 0 mM NaCl (red) and 100 mM NaCl (blue).

Before the measurements, all samples are steril-filtered (membrane-pore diameter = 0.2 μm) to eliminate large aggregates. We can therefore exclude that the spectrum is due to fibrillar structures in the CD sample. A similar effect is observed for decreasing concentrations of Cl^-. In this case, the sample was not filtered prior to the measurement. Soluble and aggregated components are therefore both present in the sample. The CD spectrum is stable on the order of 24 h, which is a prerequisite for the solution-state NMR experiments presented below. A reduction of the salt concentration from 100 to 50 mM (at a Aβ^{1-40} concentration of 0.15 mM) results in a decrease of unstructured Aβ^{1-40} in the CD spectrum (Figure 1b). Quantitative fitting of the data yields a distribution for α-helical, β-sheet, turn, and random-coil secondary-structure elements of 24.1, 37.9, 19.5, and 22.1% for 100 mM NaCl and 58.5, 15.9, 14.3, and 12.4% for 50 mM NaCl, respectively (Table 1). A high degree of α-helical structure for an intermediate oligomeric state during Aβ aggregation was observed previously (*28*). At higher peptide concentrations (0.5 mM), a similar effect is visible (Figure 1c). For the NMR experiments, conditions are employed, where Aβ^{1-40} is soluble for several days (0.5 mM Aβ^{1-40}, 50 mM phosphate, and 50 mM sodium sulfate or chloride at pH 6.9).

Table 1: Secondary-Structure Distribution for Aβ^{1-40} Dissolved in 50 mM Phosphate Buffer upon Addition of Various Salts[a]

sample	α helix (%)	β sheet (%)	turn (%)	random coil (%)
c[Aβ^{1-40}] = 0.15 mM[b]				
100 mM sulfate	34.0	34.0	17.3	17.3
100 mM perchlorate	35.9	31.9	17.1	17.4
100 mM chloride	24.1	37.9	19.5	22.1
100 mM fluoride	18.0	37.0	21.8	26.8
c[Aβ^{1-40}] = 0.15 mM[c]				
100 mM chloride (t = 0)	24.1	37.9	19.5	22.1
100 mM chloride (t = 1d)	33.8	34.2	17.1	17.2
50 mM chloride (t = 0)	48.9	23.2	13.2	14.8
50 mM chloride (t = 1d)	58.5	15.9	14.3	12.4
c[Aβ^{1-40}] = 0.50 mM[d]				
100 mM chloride	33.2	33.8	17.2	17.3

[a] In all cases, the pH was adjusted to 6.9. For the fitting of the CD curves, CDSSTR and CONTINLL were employed (*27*). [b] The dissolved peptide was filtered through a membrane with a 0.2 μm pore diameter prior to the CD measurement. [c] The dissolved peptide was directly injected into the CD cuvette without filtration. [d] The fitting of the sample containing 0 mM NaCl was omitted, because of truncation of the absorption for wavelengths below 215 nm due to the presence of aggregates.

Figure 2 shows a comparison of the ^{1}H 1D spectra that are obtained of Aβ^{1-40} dissolved in buffer containing 50 mM NaCl and 50 mM Na_2SO_4, respectively. We observe that the intensity in the spectrum of the sample containing Cl^- as the anion is reduced by a factor of 0.77. Care was taken to ensure that the same amount of peptide was in both samples. Because the error as a result of balancing errors can be estimated to be smaller than 5%, we follow that the equilibrium between soluble and insoluble Aβ^{1-40} molecules must be shifted toward the fibrillar species in the case of Cl^-. This observation is supported by the spectra presented in Figure 2b. Increasing concentrations of Cl^- yield an increase in the observed S/N ratio in the ^{1}H 1D spectra, again indicating that the equilibrium must be shifted toward a soluble monomeric structure of Aβ^{1-40} at higher salt concentrations. Interestingly, using Cl^- in the buffer, we observe a very broad peak at around 0 ppm. The intensity of this peak is increasing with decreasing salt concentrations. This resonance is not observed if we use SO_4^{2-} as the anion in the buffer (Figure 2a). We show below that the molecule giving rise to this resonance tumbles with a diffusion coefficient corresponding to a molecular weight of >100 kDa. We hypothesize that this resonance belongs to an oligomeric Aβ^{1-40} molecule, which could be identical to a critical oligomer that was postulated to be essential for fibril formation.

To estimate the molecular weight of Aβ^{1-40} under these various salt conditions, we recorded DOSY experiments. The molecular weight that we can fit to the magnetization decay curve corresponds to an average molecular weight of approximately 20.8 kDa (for SO_4^{2-}), assuming a spherical-shaped Aβ^{1-40} molecule (Figure 3). This molecular weight is larger than what is expected for a monomeric Aβ^{1-40} molecule (M = 4330 Da). The deviation can be explained

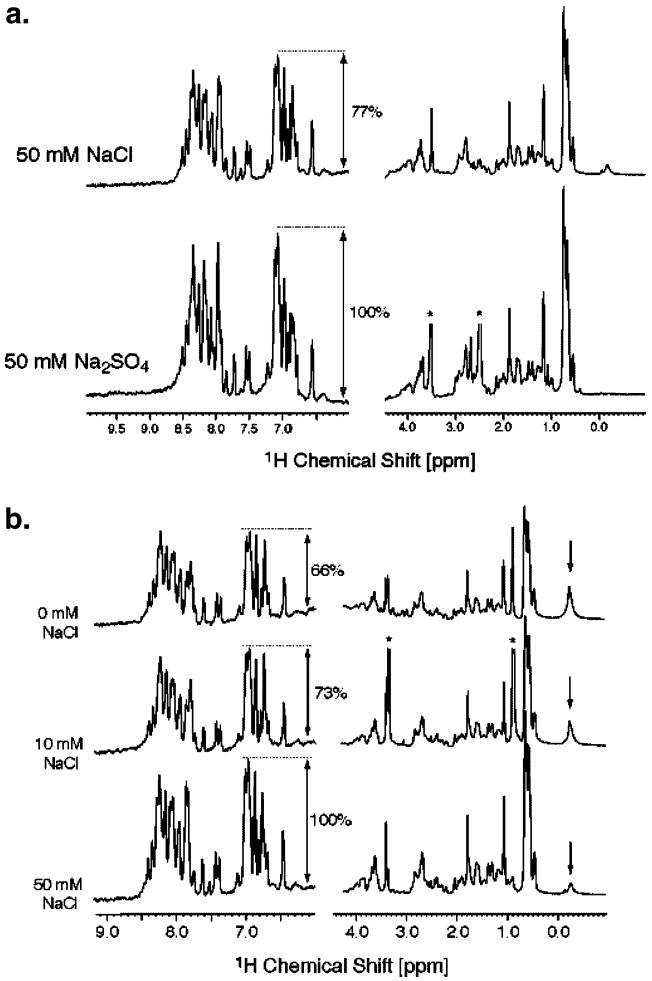

FIGURE 2: (a) ^{1}H 1D-NMR spectra of Aβ^{1-40} upon addition of 50 mM NaCl (top) and 50 mM Na_2SO_4 (bottom) to the buffer solution. The intensitiy of the sample containing NaCl is reduced by a factor of 0.77 compared to the intensity observed for the sample containing Na_2SO_4. (b) ^{1}H 1D-NMR spectra of Aβ^{1-40} at various NaCl concentrations (top, 0 mM; middle, 10 mM; bottom, 50 mM). The intensity of the resonances is increasing as the salt concentration is increased. Note that the resonance upfield of 0 ppm is increased as the NaCl concentration is decreased. The amount of peptide is the same in all samples. The error of balancing Aβ^{1-40} can be estimated to be smaller than 5%.

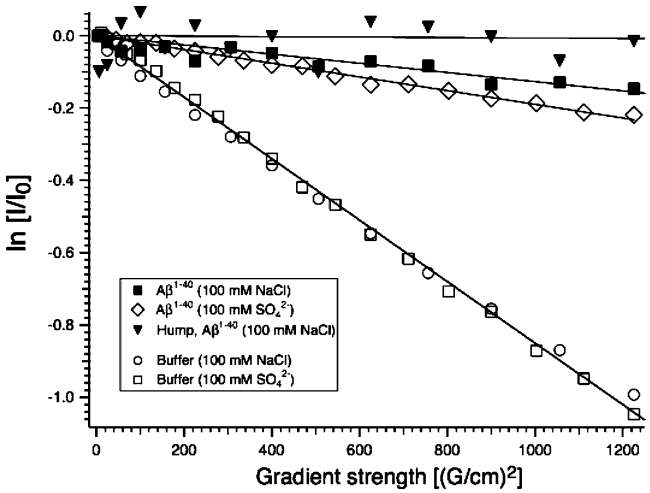

FIGURE 3: DOSY−NMR experimental data of Aβ^{1-40}. The natural logarithm of the relative intensity is represented as a function of the square of the gradient strength. Under the solution conditions used in the experiments, Aβ^{1-40} (M^{mono} = 4329.8 Da) diffuses with a molecular weight of approximately 23 900 and 20 781 Da, using 100 mM NaCl (■) and 100 mM Na_2SO_4 (◇) in the buffer solution, respectively. As a molecular weight standard, we use a resonance of oxidized β-mercaptoethanol (M = 156 Da), which is present in the buffer of the sample (○ and □). The decay of the broad resonance line at around 0 ppm, which is present in samples containing Cl^-, can be fit assuming a molecular weight of approxiamtely 14 MDa.

either by assuming that Aβ exists as an aggregated oligomer (on average, a tetramer) or by assuming that Aβ undergoes chemical exchange between a soluble and fibrillar form, yielding on average a higher molecular weight. DOSY experiments recorded for samples using 100 mM Cl^- instead of 100 mM SO_4^{2-} as the anion in the buffer solution yield a systematically higher average molecular weight in the order of ca. 24 kDa for Aβ^{1-40} (Figure 3b), supporting the hypothesis that different oligomeric states of Aβ undergo chemical exchange. Interestingly, the broad resonance at around 0 ppm diffuses with a very small diffusion constant corresponding to a molecule with an approximate molecular weight of >100 kDa.

To confirm the hypothesis that soluble Aβ^{1-40} undergoes chemical exchange with higher oligomeric state aggregates and to show that the broad resonance at around 0 ppm is related to Aβ^{1-40}, we have carried out STD−NMR experiments (Figure 4). The STD experiments are performed with an on-resonance saturation at around 0 ppm for 1.5 s. Significant STD intensities are observed for several resonances. As shown in Figure 4a, the STD intensity is dependent on the employed salt conditions in the sample. In the case of Cl^-, we observe a higher intensity in the STD experiment, even though the effective number of nuclei is smaller (reduced intensity in a reference ^{1}H 1D experiment). Especially, aromatic resonances at around 6.8 ppm are observed, which are missing in the spectrum obtained from the SO_4^{2-}-containing sample. Before performing experiments with Aβ^{1-40}, the STD experiments were carefully calibrated using two peptide samples, Sup35$^{6-25}$ and LPFFD. In both cases, the S/N ratio of the reference experiment (performed in the absence of a protein with a peptide-binding affinity) is negligible using a comparable number of scans. We assume therefore that we observe in this experiment a soluble Aβ^{1-40} molecule being in chemical exchange with a nonsoluble, aggregated Aβ^{1-40} molecule. The fibrillar state itself cannot be observed directly by solution-state NMR methods. The NMR resonances of these molecules are broadened beyond detection because of the long correlation time of an amyloid aggregate. Figure 4b represents the spectra obtained upon irradiation of the broad resonance at around 0 ppm, which we hypothetically assigned to an oligomeric state of Aβ^{1-40}. On-resonance irradiation of the broad peak induces a strong difference signal on amide, aromatic, and aliphatic resonances of Aβ^{1-40}, whereas a much weaker effect is observed in the case of off-resonance irradiation. We follow that the broad resonance must be due to a Aβ conformer, which is in chemical equilibrium with soluble Aβ^{1-40}.

To identify the chemical groups involved in Aβ^{1-40}·Aβ^{1-40} contacts, we carried out a 2D-STD−total correlation spectroscopy (TOCSY) experiment (Figure 5). The spectral assignments that have been obtained previously (*12*, *29*) could be reproduced. Figure 6a represents the aromatic

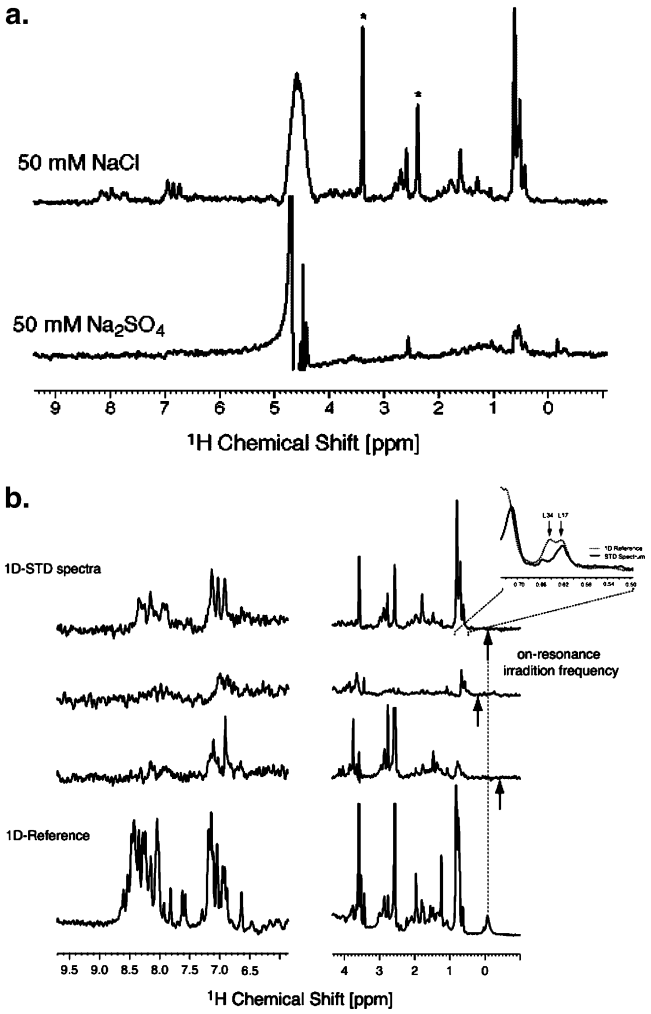

FIGURE 4: (a) ^{1}H 1D-STD spectra recorded for Aβ^{1-40} employing 50 mM NaCl (top) and Na_2SO_4 (bottom), respectively, in the buffer solution. In the case of NaCl, a higher STD signal intensity can be observed suggesting that higher oligomeric states of Aβ^{1-40} (which are not visible by solution-state NMR) undergo chemical exchange with the soluble monomeric form of Aβ^{1-40}. (b) ^{1}H 1D-STD spectra recorded for Aβ^{1-40} employing 50 mM NaCl in the buffer. The spectrum on the top is obtained after saturating the broad resonance line at 0 ppm. The spectra below are recorded after changing the on-resonance irradiation frequency as indicated by the arrow. The highest STD intensity is obtained using a saturation frequency corresponding to 0 ppm, suggesting that the molecules giving rise to this resonance are related to the soluble form of Aβ^{1-40}. For reference, a 1D ^{1}H spectrum of Aβ^{1-40} is represented on the bottom.

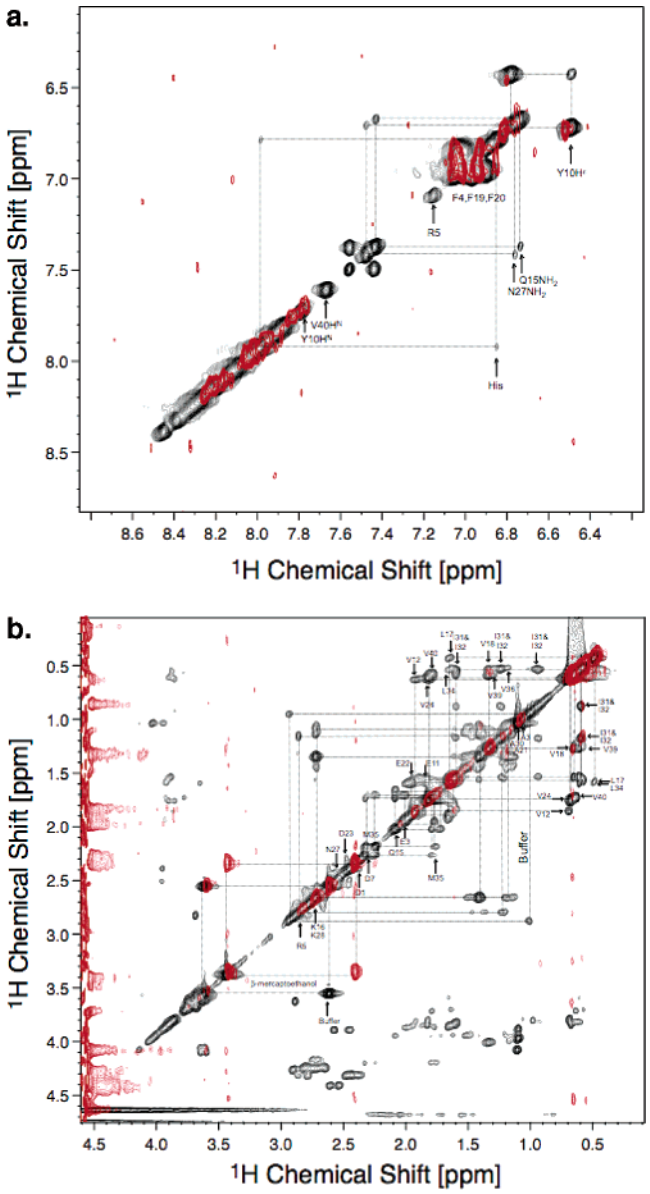

FIGURE 5: Superimposition of a 2D-STD−TOCSY of Aβ^{1-40} (red) and a standard 2D-TOCSY (black) displaying the (a) aromatic and (b) aliphatic region of the spectrum. The STD experiment yields the highest intensities for those chemical groups that are involved in interactions or chemical exchange between soluble and aggregated Aβ^{1-40} molecules.

region, and Figure 6b represents the aliphatic region of the 2D-STD−TOCSY spectrum (red), superimposed with a standard TOCSY for reference (black). We find, that mostly the methyl groups of leucine, isoleucine, valine, and alanine side chains contribute to the interaction. We observe a high STD peak intensity for the aromatic resonances of tyrosine (Y10). Careful analysis of the 1D-STD spectrum indicates that Leu-17Hδ but not Leu-34Hδ contributes to Aβ·Aβ interactions (Figure 3b). Except for Tyr-10 (Hϵ/δ), Val-18 (Hβ/Hγ), Ile-31/Ile-32 (Hγ2/Hγ1 and Hγ2/Hβ), and the buffer resonances, no STD intensity can be detected for cross peaks. An unambiguous assignment of all chemical groups that are involved in Aβ·Aβ contacts is therefore difficult and requires a uniformly ^{15}N,^{13}C-labeled Aβ^{1-40} sample. Work into this direction is currently in progress in our laboratory.

All residues that contribute to Aβ^{1-40}·Aβ^{1-40} interactions are represented in the scheme below.

D^1-**AE**<u>**F**</u>**R**HDSG<u>**Y**</u>^{10}-**EV**H*HQ*<u>**KLVFF**</u>^{20}-**AE**D***V***G*S*N<u>**K**</u>**GA**^{30}-<u>**II**</u>GLMVGGVV^{40}

Residues that can be unambiguously resolved are underlined and at the same time highlighted in bold. Alanine Hβ resonances are not resolved in the TOCSY correlation experiment. Therefore, they are represented only in bold but are not underlined. At the current resolution, it is not possible to differentiate if Glu-22Hβ or Val-12Hβ and Glu-11Hβ or Val-24Hβ contribute to the diagonal peak intensity in the STD−TOCSY experiment. At the same time, it is not possible to unambiguously assign a STD diagonal peak to lysine Hϵ (Lys-16/Lys-28) or Phe-Hβ. A similar ambiguitiy exists for the chemical shift of Arg-5-Hδ and His-Hβ. Therefore, these amino acids are represented all in bold.

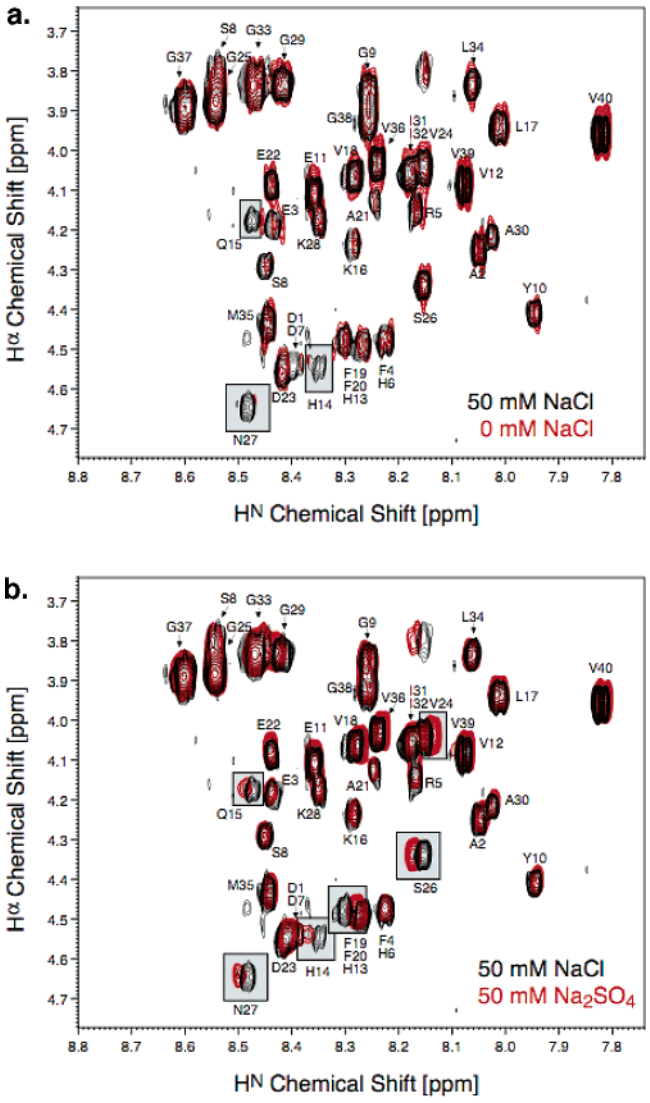

FIGURE 6: (a) Superposition of $A\beta^{1-40}$ 2D-TOCSY spectra employing 50 mM NaCl (black) and 0 mM NaCl (red) in the buffer. The H^N and H^α spectral region is displayed. Assignments are given in the figure. (b) Comparison of 2D-TOCSY spectra obtained using 50 mM NaCl (black) and 50 mM Na_2SO_4 (red) in the buffer solution.

However, we find that the region around the hydrophobic core (residues 15−24) contributes most to $A\beta^{1-40}$•$A\beta^{1-40}$ contacts.

DISCUSSION

In contrast to previous NMR studies (*29*−*32*), we find that Aβ exists in equilibrium with higher oligomeric-state structures and that the peptide appears to adopt on average a tetrameric oligomeric state. Recently, DOSY studies were carried out on the fragment $A\beta^{12-28}$ at acidic pH (2.9) (*30*). In this early study, the diffusion constant was measured as a function of the peptide concentration, to follow a shift of equilibrium from a monomeric to a dimeric $A\beta^{12-28}$. Gräslund and co-workers (*32*) investigated the same fragment ($A\beta^{12-28}$) at pH 5.0 and found that the peptide exists mostly in a monomeric, random-coil conformation. Studies by Maggio and co-workers (*31*) on the full-length peptide $A\beta^{1-40}$ show that the peptide is mostly monomeric under NMR conditions. Size-exclusion chromatography indicates, however, the population of dimeric $A\beta^{1-40}$. In this case, the peptide (0.23 mM) was directly dissolved in phosphate-buffered saline (PBS) (10 mM sodium phosphate and 100 mM NaCl at pH 7.5). We explain the different results compared to our studies by the different concentration of phosphate used in the buffer and the different peptide concentration. Similarly, Zagorski and co-workers (*29*) demonstrated that the peptide is predominantly monomeric at neutral pH. There, the sample was prepared using an explicit disaggregation protocol (*33*) to dissolve preformed fibrils and to obtain monomeric Aβ in solution.

These NMR−DOSY results obtained so far are in contrast to observations made in biochemical experiments, which indicate the presence of oligomeric structures *in vitro*. Beyreuther and co-workers observe dimeric $A\beta^{10-43}$ using size-exclusion chromatography and water as a solvent (*34*). If salt is present in the sample (e.g., 500 mM NaF), only monomeric $A\beta^{10-43}$ is observed. Variation of the anionic strength and the concentration of the salt results in a shift between lower and higher order oligomeric states. The results that we observe in our experiments follow the same trend. Further evidence that Aβ is not monomeric in solution comes from cross-linking experiments (*35*). Photoinduced cross linking of unmodified proteins (PICUP) allowed the identification of short-lived metastable assemblies. In addition, Teplow and co-workers could show that the Aβ fibril assembly proceeds *in vitro* via α-helical intermediates (*28*). The structural intermediates have an approximate molecular weight of larger than 100 kDa as estimated from dialysis experiments. Interestingly, upon addition of 50 mM NaCl, we observe a CD spectrum that contains a high degree of α-helical structure. At the same time, we observe a very broad resonance at around 0 ppm in the ^{1}H spectrum that is related to monomeric $A\beta^{1-40}$ by chemical exchange, and for that, we determined a molecular weight of >100 kDa. We speculate that the addition of anions can stabilize this transient α-helical intermediate that was observed in the process of fibril formation.

SDS-stable Aβ oligomers are as well-obtained when Aβ is either incubated in the presence of apolipoprotein J under physiological conditions (*36*) or in cell-culture medium, where the oligomeric assemblies were referred to as ADDLs (amyloid-derived diffusible ligands) (*37*, *38*). LaDu and co-workers could show that addition of 150 mM NaCl to the culture medium significantly reduces the amount of larger oligomers (*39*). At the same time, a larger number of protofibrillar structures are observed by atomic-force microscopy (AFM). A similar trend is observed in *in vitro* studies. AFM studies indicate that presence of salt yields a faster growth of fibrillar structures (*40*). We speculate that addition of salt reduces the population of oligomeric intermediate structures and this way yields larger amounts of fibrillar aggregates but also increases the population of monomeric Aβ.

In contrast to the NMR studies referred to above, we directly dissolve Aβ into buffer. In addition, we add various salts to the buffer to allow for a shift of equilibrium between different oligomeric states. To our knowledge, NMR experiments reported so far were carried out without addition of salt in the sample. The observation that we detect on average a higher oligomeric state compared to other groups is supported by the observation of a differential CD spectrum for differentially prepared samples. In the absence of salt,

the CD spectrum displays characteristic spectral features, which do not originate from random-coil structures (Figure 1).

At the same time, we do not observe a significant change in the H^N,H^α chemical-shift pattern in the presence and absence of salt (Figure 6). We can only explain this finding by assuming that higher oligomeric states are being populated, which are not detectable by solution-state NMR. This also explains the reduced signal intensity in the 1D-NMR spectra. Comparing a TOCSY correlation spectrum recorded without and with 50 mM NaCl (Figure 6a), we find that the chemical shifts of Gln-15, Asn-27, and His-14 are mostly affected. Removal of the salt induces a broadening of the respective H^N and H^α resonances resulting in the disappearance of the respective signal. We therefore speculate that the anion binds to positively charged side chains and, this way, prevents peptide−peptide interactions. A very similar result is obtained, if we compare TOCSY correlation spectra that were recorded with 50 mM NaCl and 50 mM Na_2SO_4 (Figure 6b). Again, the resonance frequency of the H^N and H^α correlation peaks of His-13, His-14, Gln-15, Val-24, Ser-26, and Asn-27 are affected. Residues that are influenced upon addition or variation of salt are represented in italics in the scheme above displaying the Aβ^{1-40} primary structure. At the same time, using Cl^- as the anion in the buffer, the aromatic resonances of His-13 and His-14 are broadened and only the cross peak involving His-6 in the aromatic part of the spectrum can be detected. The respective cross peaks are clearly visible in the SO_4^{2-} sample. This effect again might be due to the differential chemical environment of a SO_4^{2-} in contrast to a Cl^- anion. Interestingly, also Ser-26 and Asn-27 are affected. In the structure that was obtained on fibrillar Aβ^{1-40} (*17*), S26 is involved in a loop (SNKG), which is stabilized by a salt bridge between Asp-23 and Lys-28. We observe a correlation between the binding of anions to this loop and the aggregation characteristics of Aβ^{1-40}. We therefore speculate that folding and stability of this loop are influenced by the presence of anions.

Solution-state NMR structural studies revealed a collapsed-coil structure of Aβ in aqueous environment (*11*, *12*, *41*). Characteristic restraints in this structure are a nuclear Overhauser enhancement (NOE) contact between the S-methyl group of Met-35 and the side-chain and backbone atoms of Phe-19, Ala-21, and Lys-28. Furthermore, medium-range contacts between Ile-31/Ile-32 and the H^N atom of Ser-26 are observed. The side chain of Val-18 was determined to be buried within the central hydrophobic core of Aβ. Dynamic studies indicate that the central region of Aβ (residues 5−35) must adopt a relatively compact kind of molten globular state (*12*, *42*). The N- and C-terminal residues show increased mobility. In contrast, a helix-turn-helix structure was observed in aqueous SDS micellar environment (*15*), with the turn located around residues Ser-26, Asn-27, Lys-28, and Gly-29. If Aβ^{1-40} undergoes chemical exchange between a monomeric form and an oligomeric state, the NOESY correlation peaks would in fact be trNOE (*43*) correlations and should reflect the structure in the oligomeric state because of its high correlation time. Also the STD signals reflect these NOE contacts and correspond to the tertiary contacts observed in aggregated Aβ^{1-40}. In the correlation experiments that we carried out so far, we do not observe a change in the chemical-shift pattern as a function of time. Such a change would be indicative for a structural rearrangement in the course of time. At the same time, the diffusion constant measured for Aβ^{1-40} in DOSY experiments stays constant over a period of approximately 1 week (data not shown). We can therefore exclude the influence of a kinetic effect on our data.

The STD−NMR experiments give information about the aggregation mechanism of Aβ^{1-40}. We observe the largest STD peak intensities for methyl and aromatic resonances in the neighborhood of the hydrophobic core of Aβ^{1-40}. The flanking region around this hydrophobic core shows reduced STD intensities; e.g., we observe only weak intensity for Lys-Hϵ and no STD signal for Lys-Hγ/β. Because the STD peak intensity is correlated to the proximity of the respective chemical groups to the amyloid aggregates, we conclude that the region around the hydrophobic core (residues 15−24) contributes most to Aβ^{1-40}·Aβ^{1-40} intermolecular interactions. Therefore, hydrophobic interactions determine the association of Aβ monomers, before electrostatic interactions, such as the formation of salt bridges, can occur. This is in agreement with thermodynamic data, such as isothermal titration calorimetry (ITC) experiments, which show that aggregation is initially entropy-driven (*44*). The release of structured water is the driving force for self-association. Chemical-shift changes upon addition or variation of salt occur predominantly in the flanking region around the hydrophobic core residues. We observe that residues His-13, His-14, Gln-15, Val-24, Ser-26, and Asn-27 are mostly affected. We therefore conclude that anions can bind to these positively charged side chains and attenuate protein interactions by preventing attractive electrostatic interactions.

The intensities in the 1D-STD experiment recorded for Aβ dissolved in NaCl-containing buffer are significantly higher compared to the intensities that are obtained if Na_2SO_4 is present in solution. The increased STD intensity in the case of Cl^- can be explained by a decreased dissociation constant, which would allow a more efficient transfer of saturation. An exact quantitative analysis of the STD amplification factor with respect to the dissociation constant is difficult, because the saturation difference signal depends on many parameters such as temperature and proton density and requires knowledge about the intermediate aggregation states of Aβ. A detailed theoretical characterization of the STD amplification factor as a function of various experimental conditions is given by Krishna and co-workers (*45*). In theory, a comparison of STD interactions in Cl^- and SO_4^{2-} would allow for the identification of the chemical groups, which become increasingly important for aggregation, as the equilibrium is shifted toward the aggregated state. However, the intensity of the STD spectrum recorded for the SO_4^{2-}-containing sample is too low to allow unambiguous assignments of the respective resonances. These experiments require a uniformly ^{15}N,^{13}C-enriched Aβ sample. Work in this direction is currently in progess.

CONCLUSION

We have shown that Aβ^{1-40} exists under physiological conditions in different oligomeric states, which undergo chemical exchange. The equilibrium is strongly influenced by addition of anions to the solution, which allow for the shifting of the equilibrium from higher Aβ oligomeric states

to lower oligomeric states as the strength of the anion is increased. The intermediate state structure has a very high α-helical content. We find that the region around the hydrophobic core (residues 15−24) contributes most to $A\beta^{1-40}$·$A\beta^{1-40}$ contacts. The results are based on CD spectroscopy, a comparison of ^{1}H 1D spectra recorded under different salt conditions, and DOSY and STD experiments. We believe that the experiments presented can provide hints to obtain a better understanding of the mechanisms of protein−protein interactions, which lead to protein aggregation.

REFERENCES

1. Baumeister, R., and Eimer, S. (1998) Amyloid aggregates, presenilins, and Alzheimer's disease, *Angew. Chem., Int. Ed. 37*, 2978−2982.
2. Selkoe, D. J. (1999) Translating cell biology into therapeutic advances in Alzheimer's disease, *Nature 399*, A23−A31.
3. Lansbury, P. T., Jr. (1997) Structural neurology: Are seeds at the root of neuronal degeneration? *Neuron 19*, 1151.
4. Walsh, D. M., Lomakin, A., Benedek, G. B., Condron, M. M., and Teplow, D. B. (1997) Amyloid β-protein fibrillogenesis, *J. Biol. Chem. 272*, 22364−22372.
5. Walsh, D. M., Hartley, D. M., Kusumoto, Y., Fezoui, Y., Condron, M. M., Lomakin, A., Benedek, G. B., Selkoe, D. J., and Teplow, D. B. (1999) Amyloid β-protein fibrillogenesis, *J. Biol. Chem. 274*, 25945−25952.
6. Hartley, D. M., Walsh, D. M., Ye, C. P., Diehl, T., Vasquez, S., Vassilev, P. M., Teplow, D. B., and Selkoe, D. J. (1999) Protofibrillar intermediates of amyloid β-protein induce acute electrophysiological changes and progressive neurotoxicity in cortical neurons, *J. Neurosci. 19*, 8876−8884.
7. Kayed, R., Head, E., Thompson, J. L., McIntire, T. M., Milton, S. C., Cotman, C. W., and Glabe, C. G. (2003) Common structure of soluble amyloid oligomers implies common mechanism of pathogenesis, *Science 300*, 486−489.
8. Stadtman, E. (1992) Protein oxidation and aging, *Science 257*, 1220−1224.
9. Butterfield, D., Yatin, S., Varadarajan, S., and Koppal, T. (1999) Amyloid β-peptide associated free radical oxidative stress, neurotoxicity, and Alzheimer's disease, *Methods Enzymol. 309*, 746−768.
10. Varadarajan, S., Yatin, S., Aksenova, M., and Butterfield, D. A. (2000) Review: Alzheimer's amyloid β-peptide-associated free radical oxidative stress and neurotoxicity, *J. Struct. Biol. 130*, 184−208.
11. Zhang, S., Iwata, K., Lachenmann, M. J., Peng, J. W., Li, S., Stimson, E. R., Lu, Y.-A., Felix, A. M., Maggio, J. E., and Lee, J. P. (2000) The Alzheimer's peptide Aβ adopts a collapsed coil structure in water, *J. Struct. Biol. 130*, 130−141.
12. Riek, R., Günthert, P., Döbeli, H., Wipf, B., and Wüthrich, K. (2001) NMR studies in aqueous solution fail to identify significant conformational differences between the monomeric forms of two Alzheimer peptides with widely different plaque-competence, Ab(1−40)ox and Ab(1−42)ox, *Eur. J. Biochem. 268*, 5930−5936.
13. Barrow, C. J., and Zagorski, M. G. (1991) Solution structure of the β-peptide and its constituent fragments: Relation to amyloid deposition, *Science 253*, 179−182.
14. Sticht, H., Bayer, P., Willbold, D., Dames, S., Hilbich, C., Beyreuther, K., Frank, R. W., and Rösch, P. (1995) Structure of amyloid A4-(1−40)-peptide of Alzheimer's disease, *Eur. J. Biochem. 233*, 293−298.
15. Coles, M., Bicknell, W., Watson, A. A., Fairlie, D. P., and Craik, D. J. (1998) Solution structure of amyloid β-peptide(1−40) in a water-micelle environment. Is the membrane-spanning domain where we think it is? *Biochemistry 37*, 11064−11076.
16. Shao, H., Jao, S., Ma, K., and Zagorski, M. G. (1999) Solution strucutures of micelle-bound amyloid β-(1−40) and β-(1−42) peptides of Alzheimer's disease, *J. Mol. Biol. 285*, 755−773.
17. Petkova, A. T., Ishii, Y., Balbach, J. J., Antzutkin, O. N., Leapman, R. D., Delaglio, F., and Tycko, R. (2002) A structural model for Alzheimer's β-amyloid fibrils based on experimental constraints from solid-state NMR, *Proc. Natl. Acad. Sci. U.S.A. 99*, 16742−16747.
18. Mayer, M., and Meyer, B. (1999) Characterization of ligand binding by saturation transfer difference NMR spectroscopy, *Angew. Chem., Int. Ed. 38*, 1784−1788.
19. Takahashi, H., Nakanishi, T., Kami, K., Arata, Y., and Shimada, I. (2000) A novel NMR method for determining the interfaces of large protein−protein complexes, *Nat. Struct. Biol. 7*, 220−223.
20. Narayanan, S., Bösl, B., Walter, S., and Reif, B. (2003) Importance of low oligomeric weight species for prion propagation in the yeast prion system Sup35/Hsp104, *Proc. Natl. Acad. Sci. U.S.A. 100*, 9286−9291.
21. Stejskal, E. O., and Tanner, J. E. (1965) Spin diffusion measurements−Spin−echoes in the presence of a time-dependent field gradient, *J. Chem. Phys. 42*, 288.
22. Gibbs, S. J., and Johnson, C. S. (1991) A PFG NMR experiment for accurate diffusion and flow studies in the presence of eddy currents, *J. Magn. Reson. 93*, 395−402.
23. Jones, J. A., Wilkins, D. K., Smith, L. J., and Dobson, C. M. (1997) Characterisation of protein unfolding by NMR diffusion measurements, *J. Biomol. NMR 10*, 199−203.
24. Mayer, M., and Meyer, B. (2001) Group epitope mapping by saturation transfer difference NMR to identify segments of a ligand in direct contact with a protein receptor, *J. Am. Chem. Soc. 123*, 6108−6117.
25. Nakanishi, T., Miyazawa, M., Sakakura, M., Terasawa, H., Takahashi, H., and Shimada, I. (2002) Determination of the interface of a large protein complex by transferred cross-saturation measurements, *J. Mol. Biol. 318*, 245−249.
26. Goto, Y., and Aimoto, S. (1991) Anion and pH-dependent conformational transition of an amphiphilic polypeptide, *J. Mol. Biol. 218*, 387−396.
27. Sreerama, N., and Woody, R. (2000) Estimation of protein secondary structure from circular dichroism: Comparison of CONTIN, SELCON, and CDSSTR methods with an expanded reference set, *Anal. Biochem. 287*, 252−260.
28. Kirkitadze, M. D., Condron, M. M., and Teplow, D. B. (2001) Identification and characterization of key kinetic intermediates in amyloid β-protein fibrillogenesis, *J. Mol. Biol. 312*, 1103−1119.
29. Hou, L., Shao, H., Zhang, Y., Li, H., Menon, N. K., Neuhaus, E. B., Brewer, J. M., Byeon, I.-J. L., Ray, D. G., Vitek, M. P., Iwashita, T., Makula, R. A., Przybyla, A. B., and Zagorski, M. G. (2004) Solution NMR studies of the Aβ(1−40) and Aβ(1−42) peptides establish that the Met35 oxidation state affects the mechanism of amyloid formation, *J. Am. Chem. Soc. 126*, 1992−2005.
30. Mansfield, S. L., Jayawickrama, D. A., Timmons, J. S., and Larive, C. K. (1998) Measurement of peptide aggregation with pulsed-field gradient nuclear magnetic resonance spectroscopy, *Biochim. Biophys. Acta 1382*, 257−265.
31. Tseng, B. P., Esler, W. P., Clish, C. B., Stimson, E. R., Ghilardi, J. R., Vinters, H. V., Mantyh, P. W., Lee, J. P., and Maggio, J. E. (1999) Deposition of monomeric, not oligomeric, Aβ mediates growth of Alzheimer's disease amyloid plaques in human brain preparations, *Biochemistry 38*, 10424−10431.
32. Jarvet, J., Damberg, P., Bodell, K., Eriksson, L. E. G., and Gräslund, A. (2000) Reversible random coil to β-sheet transition and the early stage of aggregation of the Aβ(12−28) fragment from the Alzheimer peptide, *J. Am. Chem. Soc. 122*, 4261−4268.
33. Zagorski, M. G., Yang, J., Shao, H., Ma, K., Zeng, H., and Hong, A. (1999) Methodological and chemical factors affecting amyloid β peptide amyloidogenicitiy, *Methods Enzymol. 309*, 189−204.
34. Hilbich, C., Kisters-Woike, B., Reed, J., Masters, C. L., and Beyreuther, K. (1991) Aggregation and secondary structure of synthetic amyloid β-A4 peptides of Alzheimer's disease, *J. Mol. Biol. 218*, 149−163.
35. Bitan, G., Lomakin, A., and Teplow, D. B. (2001) Amyloid β-protein oligomerization. Prenucleation interactions revealed by photo-induced cross-linking of unmodified proteins, *J. Biol. Chem. 276*, 35176−35184.
36. Oda, T., Wals, P., Osterburg, H. H., Johnson, S. A., Pasinetti, G. M., Morgan, T. E., Rozovsky, I., Stine, W. B., Snyder, S. W., Holzman, T. F., Krafft, G. A., and Finch, C. E. (1995) Clusterin (apoJ) alters the aggregation of amyloid β-peptide (Aβ1−42) and forms slowly sedimenting Aβ complexes that cause oxidative stress, *Exp. Neurol. 136*, 22−31.

37. Lambert, M. P., Barlow, A. K., Chromy, B. A., Edwards, C., Freed, R., Liosatos, M., Morgan, T. E., Rozovsky, I., Trommer, B., Viola, K. L., Wals, P., Zhang, C., Finch, C. E., Krafft, G. A., and Klein, W. L. (1998) Diffusible, nonfibrillar ligands derived from Aβ 1−42 are potent central nervous system neurotoxins, *Proc. Natl. Acad. Sci. U.S.A. 95*, 6448−6453.
38. Gong, Y., Chang, L., Viola, K. L., Lacor, P. N., Lambert, M. P., Finch, C. E., Krafft, G. A., and Klein, W. L. (2003) Alzheimer's disease-affected brain: Presence of oligomeric A{β} ligands (ADDLs) suggests a molecular basis for reversible memory loss, *Proc. Natl. Acad. Sci. U.S.A. 100*, 10417−10422.
39. Stine, B. W., Dahlgren, K. N., Krafft, G. A., and LaDu, M. J. (2003) *In vitro* characterization of conditions for amyloid-β peptide oligomerization and fibrillogenesis, *J. Biol. Chem. 278*, 11612−11622.
40. Harper, J. D., Wong, S. S., Lieber, C. M., and Lansbury, P. T., Jr. (1999) Assembly of Aβ amyloid protofibrils: An *in vitro* model for a possible early event in Alzheimer's disease, *Biochemistry 38*, 8972−8980.
41. Zhang, S., Casey, N., and Lee, J. P. (1998) Residual structure in the Alzheimer's disease peptide: Probing the origin of a central hydrophobic cluster, *Folding Des. 3*, 413−421.
42. Massi, F., Peng, J. W., Lee, J. P., and Straub, J. E. (2001) Simulation study of the structure and dynamics of the Alzheimer's amyloid peptide congener in solution, *Biophys. J. 80*, 31−44.
43. Ni, F. (1994) Recent developments in transferred NOE methods, *Prog. NMR Spectrosc. 26*, 517−606.
44. Terzi, E., Holzemann, G., and Seelig, J. (1994) Reversible random coil-β-sheet transition of the Alzheimer β-amyloid fragment (25−35), *Biochemistry 33*, 1345−1350.
45. Jayalakshmi, V., and Krishna, N. R. (2002) Complete relaxation and conformational exchange matrix (CORCEMA) analysis of intermolecular saturation transfer effects in reversibly forming ligand−receptor complexes, *J. Magn. Reson. 155*, 106−118.

BI048264B